Bifurcations and transitions to chaos in an inverted pendulum

Sang-Yoon Kim[1,2,*] and Bambi Hu[2,3]
[1]*Department of Physics, Kangwon National University, Chunchon, Kangwon-Do 200-701, Korea*
[2]*Centre for Nonlinear Studies and Department of Physics, Hong Kong Baptist University, Hong Kong, China*
[3]*Department of Physics, University of Houston, Houston, Texas 77204*
(Received 11 February 1998)

We consider a parametrically forced pendulum with a vertically oscillating suspension point. It is well known that, as the amplitude of the vertical oscillation is increased, its inverted state (corresponding to the vertically-up configuration) undergoes a cascade of ''resurrections,'' i.e., it becomes stabilized after its instability, destabilize again, and so forth *ad infinitum*. We make a detailed numerical investigation of the bifurcations associated with such resurrections of the inverted pendulum by varying the amplitude and frequency of the vertical oscillation. It is found that the inverted state stabilizes via alternating ''reverse'' subcritical pitchfork and period-doubling bifurcations, while it destabilizes via alternating ''normal'' supercritical period-doubling and pitchfork bifrucations. An infinite sequence of period-doubling bifurcations, leading to chaos, follows each destabilization of the inverted state. The critical behaviors in the period-doubling cascades are also discussed. [S1063-651X(98)03809-4]

PACS number(s): 05.45.+b, 03.20.+i, 05.70.Jk

I. INTRODUCTION

We consider a parametrically forced pendulum, the suspension point of which undergoes a vertical periodic oscillation. The system is described by a second-order nonautonomous ordinary differential equation [1],

$$I\ddot{\theta}+b\dot{\theta}+ml(g-\epsilon\omega^2\cos\omega t)\sin\theta=0, \tag{1}$$

where the overdot denotes the differentiation with respect to time, I is the total moment of inertia, b is a damping coefficient, m is a mass attached to one end of a light rigid rod (its mass can be negligible) of length l, θ is the angular displacement measured counterclockwise from the downward vertical, and ϵ and ω are the driving amplitude and frequency of the vertical oscillation of the suspension point, respectively. Making the normalization $\omega t\rightarrow 2\pi t$ and $\theta\rightarrow 2\pi x$, we obtain a dimensionless normalized form of Eq. (1),

$$\ddot{x}+2\pi\beta\Omega\dot{x}+2\pi(\Omega^2-A\cos 2\pi t)\sin 2\pi x=0, \tag{2}$$

where $\omega_0=\sqrt{mgl/I}$, $\beta=b/I\omega_0$, $\Omega=\omega_0/\omega$, and $A=ml\epsilon/I$.

The parametrically forced pendulum has two stationary states. One is the ''normal'' state corresponding to the vertically down configuration with $x=0$, and the other one is the ''inverted'' state corresponding to the vertically up configuration with $x=\frac{1}{2}$. For the case of the ''unforced'' simple pendulum (with $A=0$), the normal state is obviously stable, while the inverted state is clearly unstable. However, as the normalized driving amplitude A is increased above a critical value, the inverted state becomes stable. This stabilization of the inverted pendulum has been discussed theoretically [2–8] and demonstrated experimentally [9–11].

Here we are interested in the bifurcations associated with the stability of the inverted state. As in the case of the normal state [12], the linear stability of the inverted state is determined by a damped Mathieu equation [13],

$$\ddot{u}+2\pi\beta\Omega\dot{u}+4\pi^2(-\Omega^2+A\cos 2\pi t)u=0. \tag{3}$$

It is well known that the Mathieu equation has an infinity of alternating stable and unstable A ranges for a given Ω [14]. Consequently, as the parameter A is increased, the inverted pendulum exhibits a cascade of ''resurrections'' (i.e., it becomes stabilized after its instability, destabilizes again and so forth *ad infinitum*) for any given Ω. By varying the normalized driving amplitude A and the normalized natural frequency Ω, we make a detailed numerical investigation of bifurcation behaviors associated with such resurrections of the inverted pendulum for a fixed value of the normalized damping coefficient β.

This paper is organized as follows. In Sec. II, we discuss bifurcations associated with the stability of periodic orbits, using the Floquet theory [15]. The bifurcation behaviors associated with the resurrections of the inverted state are then investigated through numerical calculations of its Floquet (stability) multipliers in Sec. III for the case $\beta=0.2$. It is found that the stabilizations of the inverted state occur via alternating ''reverse'' subcritical pitchfork and period-doubling bifurcations, while its destabilizations take place through alternating ''normal'' supercritical period-doubling and pitchfork bifrucations. After each destabilization of the inverted state, an infinite sequence of period-doubling bifurcations follows and leads to chaos. In Sec. IV, we also study the critical behaviors in the period-doubling cascades. Finally, a summary is given in Sec. V.

II. STABILITY, BIFURCATIONS, LYAPUNOV EXPONENTS, AND WINDING NUMBERS

In this section, we first discuss stability of periodic orbits in the Poincaré map of the parametrically forced pendulum, using the Floquet theory [15]. Bifurcations associated with

*Electronic address: sykim@cc.kangwon.ac.kr

the stability, Lyapunov exponents, and winding numbers are then discussed.

The second-order ordinary differential equation (2) is reduced to two first-order ordinary differential equations:

$$\dot{x}=y, \tag{4a}$$

$$\dot{y}=f(x,y,t)=-2\pi\beta\Omega y-2\pi(\Omega^2-A\cos 2\pi t)\sin 2\pi x. \tag{4b}$$

These equations have the (space) inversion symmetry S, because the transformation

$$S: x\to -x, \quad y\to -y, \quad t\to t \tag{5}$$

leaves Eq. (4) invariant. If an orbit $z(t)[\equiv(x(y),y(t))]$ is invariant under S, it is called a symmetric orbit. Otherwise, it is called an asymmetric orbit and has its ''conjugate'' orbit $Sz(t)$.

The surface of section for the parametrically forced pendulum is the Poincaré (time-1) map. Hence the Poincaré maps of an initial point z_0 $[=(x_0,y_0)]$ can be computed by sampling the orbit points z_m at the discrete time $t=m$ $(m=1,2,3,\ldots)$. We call the transformation $z_m\to z_{m+1}$ the Poincaré map and write $z_{m+1}=P(z_m)$.

The linear stability of a q-periodic orbit of P such that $P^q(z_0)=z_0$ is determined from the linearized-map matrix DP^q of P^q at an orbit point z_0. Here P^q means the q-times iterated map. Using the Floquet theory [15], the matrix DP^q can be obtained by integrating the linearized differential equations for small perturbations as follows.

Let $z^*(t)=z^*(t+q)$ be a solution lying on the closed orbit corresponding to the q-periodic orbit. In order to determine the stability of the closed orbit, we consider an infinitesimal perturbation $\delta z[=(u,v)]$ to the closed orbit. Linearizing Eq. (4) about the closed orbit, we obtain

$$\begin{pmatrix}\dot{u}\\ \dot{v}\end{pmatrix}=J(t)\begin{pmatrix}u\\ v\end{pmatrix}, \quad J(t)=\begin{pmatrix}0 & 1\\ f_x(x^*,t) & f_y\end{pmatrix}. \tag{6}$$

Here f_x and f_y denote the partial derivatives of $f(x,y,t)$ in Eq. (4) with respect to the variables x and y, respectively. They are given by

$$f_x(x,t)=-4\pi^2(\Omega^2-A\cos 2\pi t)\cos 2\pi x, \quad f_y=-2\pi\beta\Omega. \tag{7}$$

Note that J is a 2×2 q-periodic matrix. Let $W(t)=(w^1(t),w^2(t))$ be a fundamental solution matrix with $W(0)=I$. Here $w^1(t)$ and $w^2(t)$ are two independent solutions expressed in column vector forms, and I is the 2×2 unit matrix. Then a general solution of the q-periodic system has the following form:

$$\begin{pmatrix}u(t)\\ v(t)\end{pmatrix}=W(t)\begin{pmatrix}u(0)\\ v(0)\end{pmatrix}. \tag{8}$$

Substitution of Eq. (8) into Eq. (6) leads to an initial-value problem to determine $W(t)$

$$\dot{W}(t)=J(t)W(t), \quad W(0)=I. \tag{9}$$

It is clear from Eq. (8) that $W(q)$ is just the linearized-map matrix $DP^q(z_0)$. Hence the matrix DP^q can be obtained through integration of Eq. (9) over the period q.

The characteristic equation of the linearized-map matrix $M(\equiv DP^q)$ is

$$\lambda^2-\mathrm{tr}M\lambda+\det M=0, \tag{10}$$

where $\mathrm{tr}M$ and $\det M$ denote the trace and determinant of M, respectively. The eigenvalues, λ_1 and λ_2, of M are called the Floquet (stability) multipliers. As shown in [16], $\det M$ is calculated from a formula

$$\det M=e^{\int_0^q \mathrm{tr}J dt}. \tag{11}$$

Substituting the trace of J (i.e., $\mathrm{tr}J=-2\pi\beta\Omega$) into Eq. (11), we obtain an exact analytic result

$$\det M=e^{-2\pi\beta\Omega q}. \tag{12}$$

(Note that $\det M$ is a constant, independently of the orbits.) Accordingly, the pair of Floquet multipliers of a periodic orbit with period q lies either on the circle of radius $e^{-\pi\beta\Omega q}$ or on the real axis in the complex plane. The periodic orbit is stable only when both Floquet multipliers lie inside the unit circle. We first note that they never cross the unit circle, except at the real axis and hence Hopf bifurcations do not occur. Consequently, a stable periodic orbit can lose its stability when a Floquet multiplier decreases (increases) through -1 (1) on the real axis; conversely, an unstable periodic orbit can gain its stability when a Floquet multiplier increases (decreases) through -1 (1) on the real axis.

When a Floquet multiplier λ decreases through -1, the stable periodic orbit loses its stability via period-doubling bifurcation. On the other hand, when a Floquet multiplier λ increases through 1, it becomes unstable via pitchfork bifurcation. For each case of the period-doubling and pitchfork bifurcations, two types of supercritical and subcritical bifurcations occur. For the supercritical case of the period-doubling and pitchfork bifurcations, the stable periodic orbit loses its stability and gives rise to the birth of a new stable period-doubled orbit and a pair of new stable orbits with the same period, respectively. On the other hand, for the subcritical case of the period-doubling and pitchfork bifurcations, the stable periodic orbit becomes unstable by absorbing an unstable period-doubled orbit and a pair of unstable orbits with the same period, respectively. Hereafter, all these bifurcations, associated with instability of a stable periodic orbit, will be called the ''normal'' bifurcations. We also note that reverse processes of the normal bifurcations can occur for the case of unstable orbits. That is, when a Floquet multiplier of an unstable orbit increases (decreases) through -1 (1), it becomes stabilized via ''reverse'' period-doubling (pitchfork) bifurcations. For example, for the reverse subcritical period-doubling and pitchfork bifurcations, the unstable orbit gains its stability by emitting an unstable period-doubled orbit and a pair of unstable orbits with the same period, respectively. For more details, refer to Ref. [17].

We now discuss the Lyapunov exponent and the winding number of an orbit in the Poincaré map P. Expressing the

linearized equations (6) for the displacements in terms of the polar coordinates $u=r\cos\phi$ and $v=r\sin\phi$, we have

$$\dot{r}=r[(1+f_x)\sin\phi\cos\phi+f_y\sin^2\phi],$$

$$\dot{\phi}=-\sin^2\phi+(f_x\cos\phi+f_y\sin\phi)\cos\phi. \tag{13}$$

The motions of the displacements (r,ϕ) contain all the information about the nearby orbits. Hence we first obtain the Poincaré maps of an initial displacement (r_0,ϕ_0) by sampling the displacements (r_m,ϕ_m) at the discrete time $t=m$ $(m=1,2,3,\ldots)$. Then the average exponential rate of growth of the radius r,

$$\sigma=\lim_{m\to\infty}\frac{1}{m}\ln\frac{r_m}{r_0}, \tag{14}$$

gives the largest Lyapunov exponent σ, characterizing the average exponential rate of divergence of the nearby orbits. If σ is positive, then the orbit is called a chaotic orbit; otherwise, it is called a regular orbit. On the other hand, the average rate of increase of the angle ϕ (normalized by the factor 2π),

$$w=\lim_{m\to\infty}\frac{|\phi_m-\phi_0|}{2\pi m}, \tag{15}$$

gives the winding number w, characterizing the average rotation number of the nearby orbits during the time 1 (i.e., one iteration of P). For more details on the Lyapunov exponent and the winding number, refer to Ref. [18].

III. BIFURCATIONS OF THE INVERTED STATE AND TRANSITIONS TO CHAOS

In this section, by varying the two parameters A and Ω, we study bifurcations associated with stability of the inverted state for a damped case of $\beta=0.2$. It is well known from the theory of the Mathieu equation [14] that there exist an infinity of disconnected stability regions in the $\Omega-A$ plane (i.e., an infinity of alternating stable and unstable A ranges exist for any given Ω). Consequently, as A is increased, the inverted state undergoes a cascade of resurrections (i.e., it stabilizes after its instability, destabilizes again, and so forth *ad infinitum*) for any given Ω. We make a detailed numerical investigation of bifurcation behaviors associated with such resurrections of the inverted state.

As explained in Sec. II, the linear stability of a periodic orbit with period q in the Poincaré map P is determined from the linearized-map matrix $M(\equiv DP^q)$ of P^q. The matrix M can be obtained through numerical integration of Eq. (9) over the period q, and then its eigenvalues give the Floquet multipliers of the periodic orbit. In such a way, we determine the stability regions of the inverted state in the $\Omega-A$ plane through numerical calculations of its Floquet multipliers λ's. The first three stability regions, denoted by S_n $(n=1,2,3)$, are shown in Fig. 1. Each S_n is bounded by its lower stabilization curve, denoted by L_n, and by its upper destabilization curve, denoted by U_n. As the order n is increased, the stability region S_n becomes smaller.

We investigate bifurcation behaviors associated with the

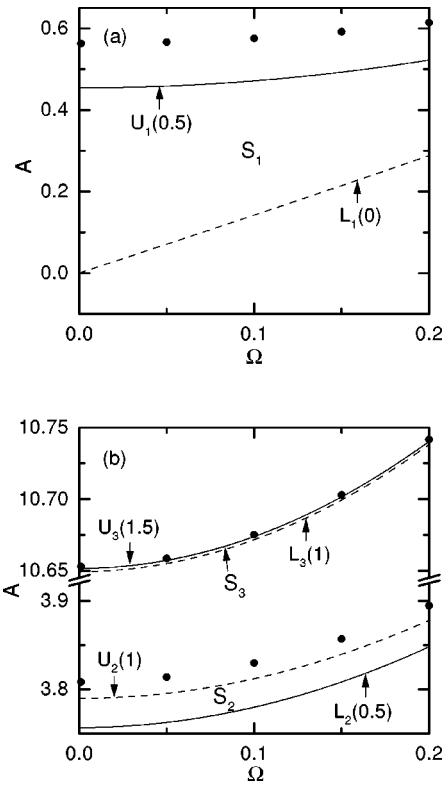

FIG. 1. Stability diagram of the inverted state in the parametrically forced pendulum. The first three stability regions of the inverted state, denoted by S_n $(n=1,2,3)$, are shown in (a) and (b). For each S_n, a period-doubling bifurcation occurs on the solid boundary curve, while a pitchfork bifurcation takes place on the dashed boundary curve. The lower and upper bifurcation curves, L_n and U_n, are also labeled by the winding numbers ω of the inverted state as $L_n(\omega)$ and $U_n(\omega)$, respectively. The accumulation points of an infinite sequence of period-doubling bifurcations, denoted by solid circles, seem to lie on the smooth critical lines. For other details, see the text.

stabilizations and destabilizations of the inverted state at the stability boundary curves in detail. It is found that they depend on whether the order n of the stability region S_n is odd or even. At the stabilization curves L_n of odd (even) n, the unstable inverted state becomes stable via reverse pitchfork (period-doubling) bifurcations. However, the situation becomes the reverse for the case of the destabilization curves U_n. That is, the stabilized inverted state loses its stability through normal period-doubling (pitchfork) bifurcations when the destabilization curves of odd (even) n are crossed. These period-doubling and pitchfork bifurcation curves are denoted by the solid and dashed curves in Fig. 1, respectively. There are two types of supercritical and subcritical bifurcations for the case of the period-doubling and pitchfork bifurcations, as explained in Sec. II. All the stabilizations occur via the subcritical bifurcations, while all the destabilizations take place through the supercritical bifurcations. Consequently, with increasing A the inverted state stabilizes via alternating reverse subcritical pitchfork and period-doubling bifurcations, while it destabilizes through alternating normal supercritical period-doubling and pitchfork bifurcations. After each destabilization of the inverted state, an infinite sequence of period-doubling bifurcations, leading to chaos, also follows and ends at a finite accumulation point.

We obtain such accumulation points for several values of Ω ($\Omega = 0.001, 0.05, 0.1, 0.15, 0, 2$). They are denoted by solid circles in Fig. 1 and seem to lie on smooth critical lines. When crossing these critical lines, period-doubling transitions to chaos occur.

The lower and upper bifurcation curves, L_n and U_n, in Fig. 1 are also labeled by the winding numbers ω of the inverted state as $L_n(\omega)$ and $U_n(\omega)$, respectively. We obtain the winding number ω of the inverted state through numerical integration of the linearized equation (13) over period 1. It is known that, for the pitchfork bifurcations, the winding numbers of the inverted state become integers, while they are odd multiples of 1/2 for the period-doubling bifurcations [18]. Note that the winding number ω of the inverted state increases with respect to the order n of the bifurcation curves.

We now present the concrete examples of bifurcations associated with the resurrections of the inverted state for the case $\Omega = 0.1$. The bifurcation diagrams and the phase-flow and Poincaré-map plots are also given for clear presentation of the bifurcations. We first investigate the bifurcation behaviors associated with the first resurrection of the inverted state with increasing A. For the unforced case of $A = 0$, the inverted state is clearly unstable. However, when the lower stabilization curve L_1 of the first stability region S_1 is crossed at the first stabilization point $A_s(1) = 0.142\,066\ldots$, the unstable inverted state becomes stabilized via reverse subcritical pitchfork bifurcation. The bifurcation diagram near the first resurrection of the inverted state is shown in Fig. 2(a). Through the reverse subcritical pitchfork bifurcation, a conjugate pair of unstable asymmetric orbits with period 1 appears, and their phase portraits for $A = 0.15$ are shown in Fig. 2(b). However, when the upper destabilization curve U_1 of S_1 is crossed at the first destabilization point $A_d(1) = 0.471\,156\ldots$, the stabilized inverted state loses its stability via normal supercritical period-doubling bifurcation. Consequently, a stable period-doubled symmetric orbit appears and its phase portrait for $A = 0.5$ is also shown in Fig. 2(c). Note that the winding number ω of the inverted state increases from 0 to 1/2, as A is changed from $A_s(1)$ to $A_d(1)$. We also study the subsequent bifurcations with increasing A further. Unlike the case of the inverted state, the symmetric 2-periodic orbit becomes unstable by a symmetry-breaking pitchfork bifurcation, which leads to the birth of a conjugate pair of stable asymmetric orbits with period 2. Then each 2-periodic orbit with broken symmetry undergoes an infinite sequence of period-doubling bifurcations, ending at its accumulation point A_1^* ($= 0.575\,154\ldots$). Consequently, a period-doubling transition to chaos occurs when the parameter A increases through A_1^*. The critical scaling behaviors of period doublings near the critical point A_1^* are the same as those for the 1D maps, as will be seen in Sec. IV.

With a further increase of A, we also study the bifurcations associated with the second resurrection of the inverted state. Since the order of S_2 is even, the types of bifurcations associated with the stabilization and destabilization become different from those for the case of the first resurrection. When the lower stabilization curve L_2 of S_2 is crossed at the second stabilization point $A_s(2)$ ($= 3.779\,771\ldots$), a reverse subcritical period-doubling bifurcation occurs, which is in contrast to the case of the first resurrection. Consequently, the unstable inverted state stabilizes with the birth of a new unstable symmetric orbit with period 2. Figure 3(a) shows the bifurcation diagram in the vicinity of this second resurrection. The phase portrait of the newly born unstable symmetric 2-periodic orbit for $A = 3.783$ is also shown in Fig. 3(b). However, when the upper destabilization curve U_2 of S_2 is crossed at the second destabilization point $A_d(2) = 3.811\,973\ldots$, a normal supercritical pitchfork bifurcation occurs, which is also in contrast to the case of the first destabilization. As a result, the stable inverted state destabilizes with the birth of a conjugate pair of stable asymmetric orbits of period 1. The phase portraits of the newly-born stable asymmetric orbits with period 1 for $A = 3.815$ are shown in Fig. 3(c). Note that the winding number ω also increases from 1/2 to 1, as A is varied from $A_s(2)$ to $A_d(2)$. As A is

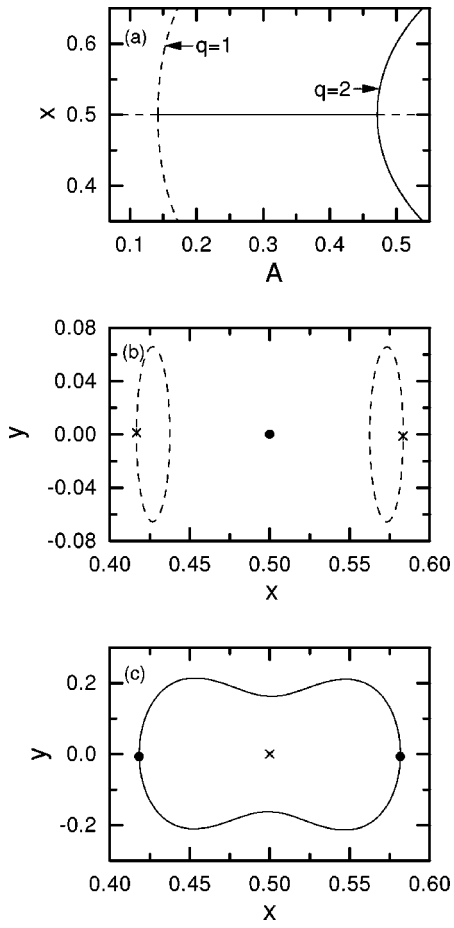

FIG. 2. (a) Bifurcation diagram (plot of x vs A) in the vicinity of the first resurrection of the inverted state. Here the solid and dashed lines denote stable and unstable orbits, respectively, and q denotes the period of an orbit. (b) Phase portraits for $A = 0.15$. The stabilized inverted state is denoted by the solid circle. On the other hand, the phase flows of a conjuate pair of unstable orbits with period 1 born via reverse subcritical pitchfork bifurcation are denoted by dashed curves, and their Poincaré maps are represented by the crosses. (c) Phase portraits for $A = 0.5$. The destabilized inverted state is denoted by the cross. On the other hand, the phase flow of a stable orbit with period 2 born via normal supercritical period-doubling bifurcation is denoted by a solid curve, and its Poincaré maps are represented by the solid circles.

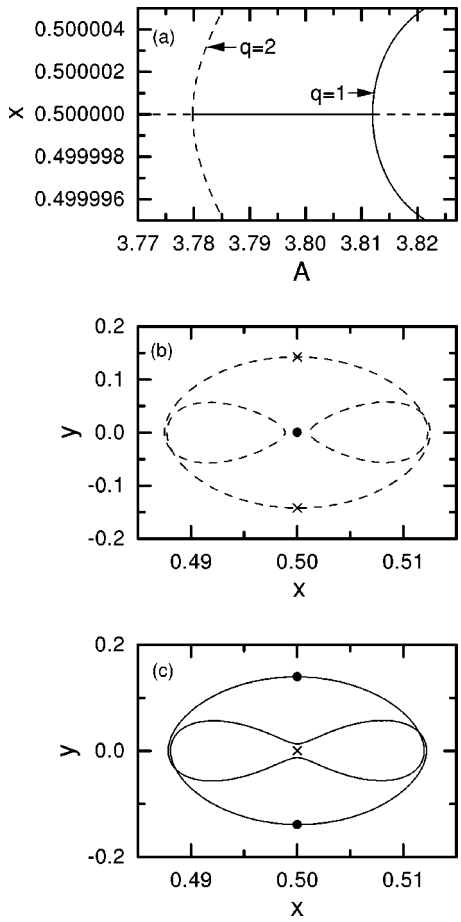

FIG. 3. (a) Bifurcation diagram near the second resurrection of the inverted state. The solid and dashed lines and q represent the same as those as in Fig. 1. (b) Phase portraits for $A=3.783$. The stabilized inverted state is denoted by the solid circle. On the other hand, the phase flow of an unstable orbit with period 2 born via reverse subcritical period-doubling bifurcation is denoted by a dashed curve, and its Poincaré maps are represented by the crosses. (c) Phase portraits for $A=3.815$. The destabilized inverted state is designated by the cross. On the other hand, the phase flows of a conjugate pair of stable asymmetric orbits with period 1 born via normal supercritical pitchfork bifurcation are denoted by solid curves, and their Poincaré maps are represented by the solid circles.

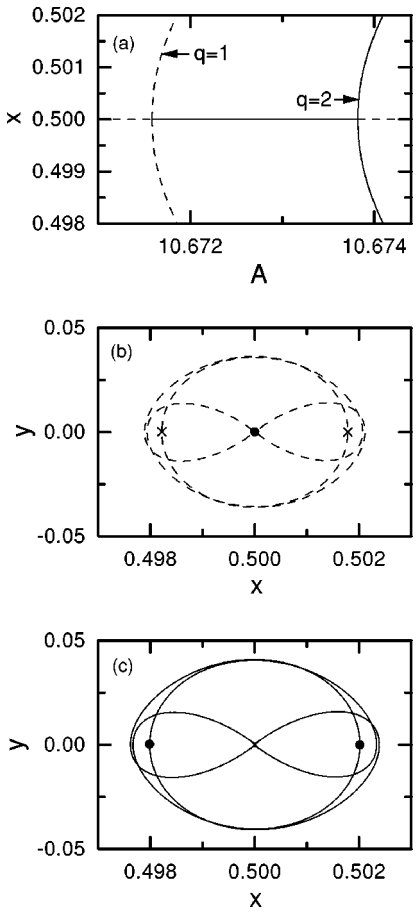

FIG. 4. (a) Bifurcation diagram near the third resurrection of the inverted state. The solid and dashed lines and q denote the same as those in Fig. 1. Note that the bifurcation behaviors associated with the stabilization and destabilization of the inverted state are the same as in Fig. 1. The phase portraits of the orbits associated with the stabilization and destabilization are shown in (b) and (c) for $A=10.6718$ and 10.6741, respectively. For other details see the text.

further increased, a second infinite sequence of period-doubling bifurcations, leading to chaos, also follows and ends at its accumulation point A_2^* $(=3.829\,784\ldots)$. The critical scaling behaviors of period doublings near $A=A_2^*$ are the same as those near the first accumulation point A_1^*.

Finally, we investigate the bifurcations associated with the third resurrection of the inverted state. The types of bifurcations associated with the stabilization and destabilization become the same as those for the case of the first resurrection, because the order of S_3 is odd. As shown in Fig. 4(a), the unstable inverted state stabilizes with the birth of a conjugate pair of unstable asymmetric orbits with period 1 via reverse subcritical pitchfork bifurcation at the third stabilization point $A_s(3)$ $(=10.671\,579\ldots)$ on the lower stabilization curve L_3. As A is increased, the stable inverted state also destabilizes with the birth of a stable period-doubled symmetric orbit through a normal supercritical period-doubling bifurcation at the third destabilization point $A_d(3)$ $(=10.673\,818\ldots)$ on the upper destabilization curve U_3. The phase portraits of the newly-born orbits for the cases of the stabilization and destabilization are shown in Figs. 4(b) and 4(c) for $A=10.6718$ and 10.6741, respectively. We also note that, as A is changed from $A_s(3)$ to $A_d(3)$, the winding number ω increases from 1 to 3/2. Since the winding number of the inverted state increases, its nearby orbits have an increasing number of loops [e.g., compare Figs. 4(b) and 4(c) with Figs. 2(b) and 2(c)]. The subsequent bifurcation behaviors are also the same as those for the above first case. Consequently, a third infinite sequence of period-doubling bifurcations, leading to chaos, follows and ends at its accumulation point A_3^* $(=10.675\,090\ldots)$. The critical scaling behaviors of period doublings are also the same as those near A_1^*.

IV. CRITICAL BEHAVIORS IN THE PERIOD-DOUBLING CASCADES

In this section, we first investigate the winding-number sequence of the period-doubling cascade and find that the winding numbers at the period-doubling bifurcation points constitute an alternating sequence converging to a limit

value, as in other oscillators [18]. The orbital scaling behavior and the power spectra of the periodic orbits born via period-doubling bifurcations as well as the parameter scaling behaviors are then investigated. These critical scaling behaviors for all cases studied are found to be the same as those of the 1D maps [19].

As an example, we consider the case $\Omega=0.1$. The first three accumulation points A_i^*'s ($i=1,2,3$) of the period-doubling bifurcations are shown in Fig. 1. Only the critical behaviors at the first accumulation point A_1^* are given below, because the critical behaviors at all the three accumulation points are the same. For this first case, we follow the periodic orbits of period 2^k up to level $k=8$. As explained in Sec. III, the stabilized inverted state loses its stability for $A=A_d(1)$ through a normal supercritical period-doubling bifurcation, giving rise to the birth of a stable period-doubled symmetric orbit. However, this symmetric 2-periodic orbit becomes unstable via symmetry-breaking pitchfork bifurcation, which results in the birth of a conjugate pair of asymmetric orbits with period 2. Then each 2-periodic orbit with broken symmetry undergoes an infinite sequence of period-doubling bifurcations, ending at its accumulation point A_1^*. Therefore, a period-doubling transition to chaos takes place when the parameter A increases through A_1^*.

Figure 5(a) shows the bifurcation diagram of the first period-doubling cascade. [For the sake of convenience, only one asymmetric orbit of period 2 is shown in Fig. 5(a).] The largest Lyapunov exponent σ and the winding number ω in the period-doubling cascade are also given in Figs. 5(b) and 5(c), respectively. The largest Lyapunov exponent has a constant value ($=-\pi\beta\Omega$) when the Floquet multipliers λ's lie on the circle of radius $e^{-\pi\beta\Omega q}$ (in the complex plane), while it changes smoothly when λ's lie on the real axis. The value of σ becomes zero at each period-doubling bifurcation point. Unlike the case of σ, the winding number ω takes a constant rational value when λ's lie on the real axis, and hence it can change only when λ's lie on the circle of radius $e^{-\pi\beta\Omega q}$. Consequently, $\omega(A)$ becomes a steplike function. Rational steps appear near the period-doubling bifurcation points, as shown in Fig. 5(c). The sequence of the winding-number steps is given by $\omega_k=\frac{1}{6}[1-(-1)^k/2^k]$ $k=1, 2, \ldots$); the first three values (corresponding to $k=1$, 2, and 3) are given in Fig. 5(c). Note that the winding numbers constitute an alternating sequence converging to its limit value $\omega_\infty^{(1)}$ ($=1/6$). Consequently, the quasiperiodic attractor at the first accumulation point A_1^* has the winding number $\omega_\infty^{(1)}$. We also study the winding-number sequences in the second and third period-doubling cascades. They are given by $\omega_k=\frac{1}{3}[2+(-1)^k/2^k]$ and $\omega_k=\frac{1}{6}[7-(-1)^k/2^k]$, respectively. As in the first case, these alternating sequences also converge to their limit values $\omega_\infty^{(2)}$ ($=2/3$) and $\omega_\infty^{(3)}$ ($=7/6$). Hence, the quasiperiodic attractors at the second and third accumulation points A_2^* and A_3^* have their winding numbers $\omega_\infty^{(2)}$ and $\omega_\infty^{(3)}$, respectively. Note that the winding numbers $\omega_\infty^{(i)}$ of the quasiperiodic attractors at the accumulation points A_i^* increase with i.

Table I gives the A values at which the period-doubling bifurcations occur; at A_k, a Floquet multiplier of an asymmetric orbit with period 2^k becomes -1. The sequence of

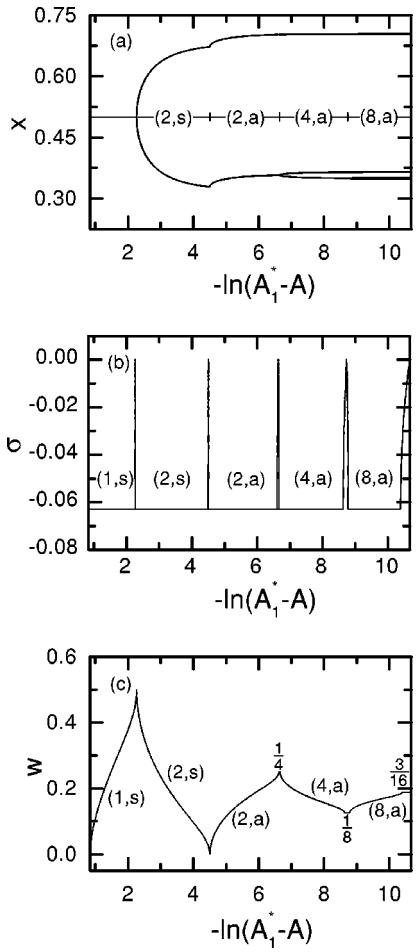

FIG. 5. (a) Bifurcation diagram [plot of x vs $-\ln(A_1^*-A)$] of the first period-doubling cascade, (b) plot of the largest Lyapunov exponent σ vs $-\ln(A_1^*-A)$, and (c) plot of the winding number ω vs $-\ln(A_1^*-A)$ for $\Omega=0.1$. Here (q, s, or a) denotes the stable A range of the symmetric or asymmetric orbit with period q.

A_k converges geometrically to its limit value A_1^* with an asymptotic ratio δ:

$$\delta_k=\frac{A_k-A_{k-1}}{A_{k+1}-A_k}\rightarrow\delta. \tag{16}$$

The sequence of δ_k is also listed in Table I. Note that its limit value δ ($\simeq 4.7$) agrees well with that ($=4.669\cdots$) for

TABLE I. Asymptotically geometric convergence of the parameter sequence $\{A_k\}$.

k	A_k	δ_k
1	0.573 847 671 035	
2	0.574 992 231 118	8.26
3	0.575 130 862 947	7.25
4	0.575 149 971 647	5.68
5	0.575 153 335 892	4.78
6	0.575 154 039 822	4.65
7	0.575 154 191 110	4.69
8	0.575 154 223 350	

TABLE II. Asymptotically geometric convergence of the orbital sequences $\{x^{(k)}\}$ and $\{y^{(k)}\}$.

k	$x^{(k)}$	$\alpha_{x,k}$	$y^{(k)}$	$\alpha_{y,k}$
1	0.356 951 938		0.014 184 290	
2	0.349 165 197	−4.016	0.014 680 027	−6.189
3	0.351 104 216	−3.547	0.014 599 925	−2.709
4	0.350 557 529	−3.078	0.014 629 491	−3.543
5	0.350 735 119	−2.608	0.014 621 145	−2.409
6	0.350 667 034	−2.509	0.014 624 610	−2.615
7	0.350 694 173	−2.502	0.014 623 285	−2.448
8	0.350 683 324		0.014 623 826	

the 1D maps [19]. We also obtain the value of A_1^* $(=0.575\,154\,232\ldots)$ by superconverging the sequence of $\{A_k\}$ [20].

As in the 1D maps, we are also interested in the orbital scaling behavior near the most rarified region. Hence we first locate the most rarified region by choosing an orbit point $z^{(k)}$ $[=(x^{(k)},y^{(k)})]$ that has the largest distance from its nearest orbit point $P^{2^{k-1}}(z^{(k)})$ for $A=A_k$. The two sequences $\{x^{(k)}\}$ and $\{y^{(k)}\}$, listed in Table II, converge geometrically to their limit values x^* and y^* with the 1D asymptotic ratio α $(=-2.502\cdots)$, respectively:

$$\alpha_{x,k}=\frac{x^{(k)}-x^{(k-1)}}{x^{(k+1)}-x^{(k)}}\to\alpha,\quad \alpha_{y,k}=\frac{y^{(k)}-y^{(k-1)}}{y^{(k+1)}-y^{(k)}}\to\alpha. \tag{17}$$

The values of x^* $(=0.350\,686\ldots)$ and y^* $(=0.014\,623\ldots)$ are also obtained by superconverging the sequences of $x^{(k)}$ and $y^{(k)}$, respectively.

We finally study the power spectra of the 2^k-periodic orbits at the period-doubling bifurcation points A_k. Consider the orbit of level k whose period is $q=2^k$, $\{z_m^{(k)}=(x_m^{(k)},y_m^{(k)}),\ m=0,1,\ldots,q-1\}$. Then its Fourier component of this 2^k-periodic orbit is given by

$$z^{(k)}(\omega_j)=\frac{1}{q}\sum_{m=0}^{q-1} z_m^{(k)} e^{-i\omega_j m}, \tag{18}$$

where $\omega_j=2\pi j/q$, and $j=0,1,\ldots,q-1$. The power spectrum $P^{(k)}(\omega_j)$ of level k defined by

$$P^{(k)}(\omega_j)=|z^{(k)}(\omega_j)|^2 \tag{19}$$

has discrete peaks at $\omega=\omega_j$. In the power spectrum of the next $(k+1)$ level, new peaks of the $(k+1)$th generation appear at odd harmonics of the fundamental frequency, $\omega_j=2\pi(2j+1)/2^{(k+1)}$ $(j=0,\ldots,2^k-1)$. To classify the contributions of successive period-doubling bifurcations in the power spectrum of level k, we write

$$P^{(k)}=P_{00}\delta(\omega)+\sum_{l=1}^{k}\sum_{j=0}^{2^{(l-1)}-1} P_{lj}^{(k)}\delta(\omega-\omega_{lj}), \tag{20}$$

where $P_{lj}^{(k)}$ is the height of the jth peak of the lth generation appearing at $\omega=\omega_{lj}$ $(\equiv 2\pi(2j+1)/2^l)$. As an example, we

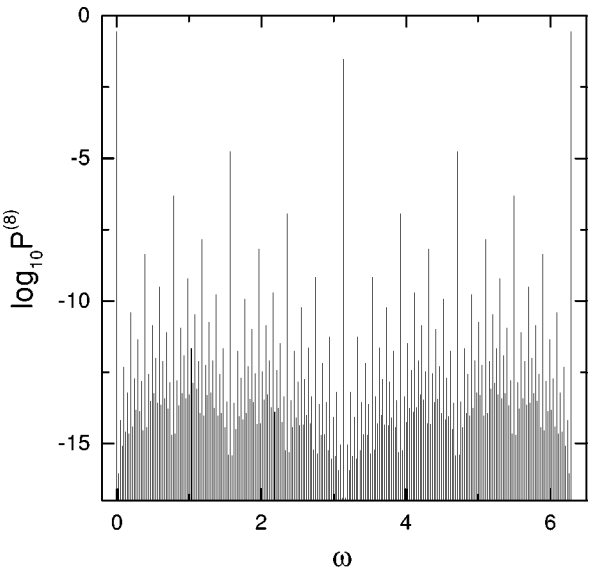

FIG. 6. Power spectrum $P^{(8)}(\omega)$ of level 8 for $A=A_8$ $(=0.575\,154\,223\,350)$.

consider the power spectrum $P^{(8)}(\omega)$ of level 8 shown in Fig. 6. The average height of the peaks of the lth generation is given by

$$\phi^{(k)}(l)=\frac{1}{2^{(l-1)}}\sum_{j=0}^{2^{l-1}-1} P_{lj}^{(k)}. \tag{21}$$

It is of interest whether or not the sequence of the ratios of the successive average heights

$$2\beta^{(k)}(l)=\phi^{(k)}(l)/\phi^{(k)}(l+1), \tag{22}$$

converges. The ratios are listed in Table III. They seem to approach a limit value, $2\beta\simeq 21$, which also agrees well with that $(=20.96\cdots)$ for the 1D maps [21].

V. SUMMARY

We carried out a detailed investigation of bifurcations associated with resurrections of the inverted state through numerical calculations of its Floquet multipliers. It was found that its stabilizations occur via alternating reverse subcritical pitchfork and period-doubling bifurcations, while its destabilizations take place through alternating normal supercritical

TABLE III. Sequence $2\beta^{(k)}(l)$ $[\equiv\phi^{(k)}(l)/\phi^{(k)}(l+1)]$ of the ratios of the successive average heights of the peaks in the power spectra

k	l			
	4	5	6	7
6	34.7	24.6		
7	34.0	24.5	21.7	
8	33.9	24.0	21.7	21.5

period-doubling and pitchfork bifurcations. An infinite sequence of period-doubling bifurcations, leading to chaos, also follows each destabilization of the inverted state. The orbital and parameter scaling behaviors near the accumulation points A_i^* of the period-doubling cascades are also found to be the same as those of the 1D maps, although the winding numbers $\omega_\infty^{(i)}$ of the quasiperiodic attractors at the accumulation points increase with i.

ACKNOWLEDGMENTS

Some part of this work has been done while S.Y.K. visited the Center for Nonlinear Studies of the Hong Kong Baptist University. This work was supported by the Basic Science Research Institute Program, Ministry of Education, Korea, under Project No. BSRI-97-2401 (S.Y.K.) and in part by grants from the Hong Kong Research Grants Council (RGC) and the Hong Kong Baptist University Faculty Research Grant (FRG).

[1] L. D. Landau and E. M. Lifshitz, *Mechanics* (Pergamon, New York, 1976), p. 80; V. I. Arnold, *Mathematical Methods of Classical Mechanics* (Springer-Verlag, New York, 1978), p. 113.

[2] H. C. Corben and P. Stehle, *Classical Mechanics*, 2nd ed. (Wiley, New York, 1960), p. 67.

[3] P. L. Kapitza, in *Collected Papers of P. L. Kapitza*, edited by D. Ter Haar (Pergamon, London, 1965), p. 714.

[4] J. J. Stoker, *Nonlinear Vibrations in Mechanical and Electrical Systems* (Interscience, New York, 1966), p. 189.

[5] L. D. Landau and E. M. Lifshitz, *Mechanics* (Pergamon, New York, 1976), p. 93.

[6] V. I. Arnold, *Mathematical Methods of Classical Mechanics* (Ref. [1]), p. 121.

[7] M. Levi, SIAM (Soc. Ind. Appl. Math.) Rev. **30**, 639 (1988).

[8] J. A. Blackburn, H. J. T. Smith, and N. Grønbech-Jensen, Am. J. Phys. **60**, 903 (1992).

[9] M. H. Friedman, J. E. Campana, L. Kelner, E. H. Seeliger, and A. L. Yergey, Am. J. Phys. **50**, 924 (1982)

[10] M. M. Michaelis, Am. J. Phys. **53**, 1079 (1985).

[11] H. J. T. Smith and J. A. Blackburn, Am. J. Phys. **60**, 909 (1992).

[12] S.-Y. Kim and K. Lee, Phys. Rev. E **53**, 1579 (1996); J. B. McLaughlin, J. Stat. Phys. **24**, 375 (1981).

[13] The sign in front of Ω^2 in Eq. (3) is different for the normal and inverted states. For the case of the normal state the sign is positive, while it is minus for the case of the inverted state. The sign is important, because it affects the stability.

[14] P. M. Morse and H. Feshbach, *Methods of Theoretical Physics* (McGraw-Hill, New York, 1953), Sec. 5.2; J. Mathews and R. L. Walker, *Mathematical Methods of Physics* (Benjamin, New York, 1965), Sec. 7.5.

[15] S. Lefschetz, *Differential Equations: Geometric Theory* (Dover, New York, 1977), Sec. 3.5.

[16] S. Lefschetz, *Differential Equations: Geometric Theory* (Ref. [15]), p. 60. See Eq. (4.3).

[17] J. Guckenheimer and P. Holmes, *Nonlinear Oscillations, Dynamical Systems, and Bifurcations of Vector Fields* (Springer-Verlag, New York, 1983), Sec. 3.5.

[18] U. Parlitz, Int. J. Bifurcation Chaos Appl. Sci. Eng. **3**, 703 (1993), and references therein.

[19] M. J. Feigenbaum, J. Stat. Phys. **19**, 25 (1978); **21**, 669 (1979).

[20] R. S. MacKay, Ph.D. thesis, Princeton University, 1982. See Eqs. (3.1.2.12) and (3.1.2.13).

[21] M. Nauenberg and J. Rudnick, Phys. Rev. B **24**, 493 (1981).